Method to Determine Compressive Bending Performance in Static and Fatigue Loading for Pediatric Non-Fusion Devices

A Thesis
SUBMITTED TO THE FACULTY OF THE
UNIVERISTY OF MINNESOTA
BY

Mary H. Foltz

IN PARTIAL FULFILLMENT OF THE
REQUIREMENTS
FOR THE DEGREE OF
MASTER OF SCIENCE

ADVISOR
Dr. Victor H. Barocas
CO-ADVISOR
Dr. Joan E. Bechtold

January 2016

ABSTRACT

Background: Early onset scoliosis is a three-dimensional deformity of the spine and trunk – diagnosed before the age of 10 – and occurs in 3 to 5 out of 100,000 infant and juvenile populations. Surgical intervention is often necessary for pediatric patients with severe curvatures. During these procedures, spinal growing rods – known as pediatric non-fusion devices – are placed in the patients to allow for spinal growth. Growing-rod constructs have a high failure rate due to larger demands on the rods as no fusion is performed and the rods are continually loaded. The constructs are serially lengthened at 6-month intervals placing additional demands on the construct. Currently, there are no standards on how to develop and utilize a finite element model – to predict durability of commonly used constructs within the patient.

Methods: Finite element models representing static compression bending were implemented using Abaqus CAE (Dassault Systemés Simulia Corporation, Providence, Rhode Island). The material properties used were based on ASTM standard 1537 and 136. The models were created with C3D8R type elements. The model applied a controlled displacement until failure or contact occurred between the superior and inferior UHMWPE blocks. Failure was defined as the point at which permanent deformation of the construct occurs, due to fracture, plastic deformation, or slip. Eight constructs were analyzed based on the rod material (titanium/cobalt chrome), active length (76-/376-mm), and construct type (F1717/growing-rod).

Results: The force-displacement curves and maximum principle stress for each whole model were evaluated. The longer active lengths required smaller forces for failure. Growing-rod constructs required smaller forces and displacements to failure compared to F1717 constructs. Failure at the pedicle screw head was found on each model.

Conclusions: A new ASTM standard for growing-rod constructs should be created based off of a longer active length, the overlap of the rod connectors, and location of the rod connectors. FE model provides insight into failure mechanisms not otherwise apparent in clinical settings.

Table of Contents

List of Tables

List of Figures

List of Abbreviations

ASM	Aerospace Specification Metals, Inc.
ASTM	American Society for Testing and Materials
EOS	Early Onset Scoliosis
FE	Finite Element
MSI	Minnesota Supercomputing Institute
UHMWPE	Ultrahigh Molecular Weight Polyethylene

List of Notations

mm	Millimeter
N	Newton
MPa	Mega-Pascal (i.e. N/mm^2)

Chapter 1. INTRODUCTION

1.1 – Scoliosis

Scoliosis (Figure 1) is a three-dimensional deformity of the spine and trunk that affects individuals of all ages. Early onset scoliosis (EOS) is defined as scoliosis diagnosed in individuals under the age of 10 years, and occurs in 0.003% to 0.005% of the population (Scoliosis Research Society, 2015). When the Cobb angle – the angle found between the lines drawn from the endplates of the end vertebrae (Figure 2) – surpasses 10°, then the curve is considered to be scoliotic (Scoliosis Research Society, 2015).

Figure 1 - Scoliosis (Mayo Foundation for Medical Education and Research, 2015)

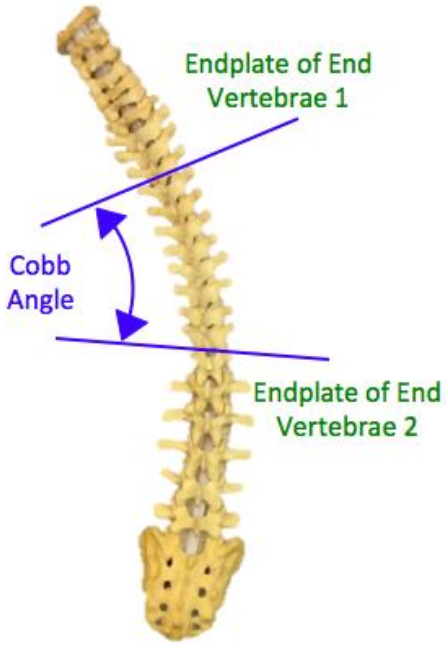

Figure 2 - Cobb Angle

The effects of scoliosis include but are not limited to back pain, diminished lung function, stiffness of the rib cage, and mortality due to respiratory failure or cardiovascular disease (Pehrsson, Larsson, Oden, & Nachemson, 1992). *Pehrsson* found that there is a statistically significant increase in mortality due to respiratory failure in EOS patients. Surgical and non-surgical interventions are known to slow, stop, and/or reverse the Cobb angle (Figure 3). Non-surgical interventions include observation for Cobb angles under 25° and bracing for curves between 25° and 50°; surgical intervention is considered when the Cobb angle is greater than 50°. Surgical interventions are a last resort, being recommended only after a multitude of factors have been considered. The two major factors on which the surgeon assesses the need for surgery are (1) age and (2) severity of Cobb angle. (Scoliosis Research Society, 2015)

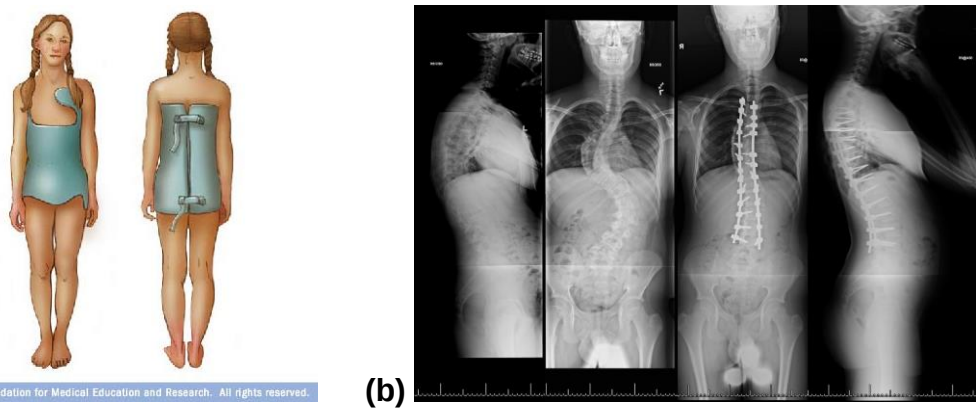

Figure 3 - Treatment, (a) Brace (Mayo Foundation for Medical Education and Research, 2015) and (b) Surgery

The mechanics for adult and early-onset scoliosis patients require specific needs accounting for the maturity of the spine.

1.2 – Current Knowledge and Design – Adult

Adult scoliosis surgery generally consists of spinal fusion accompanied by mechanical implants to correct the scoliotic Cobb angle. Fusion of the spine is done by removing the vertebral disc and inserting a bone graft – the graft is harvested during surgery when using autograft or before surgery for allografts – into the intervertebral area fusing the two vertebrae together. For scoliosis fusion, mechanical implants assist the fusion in correction. (Scoliosis Research Society, 2015)

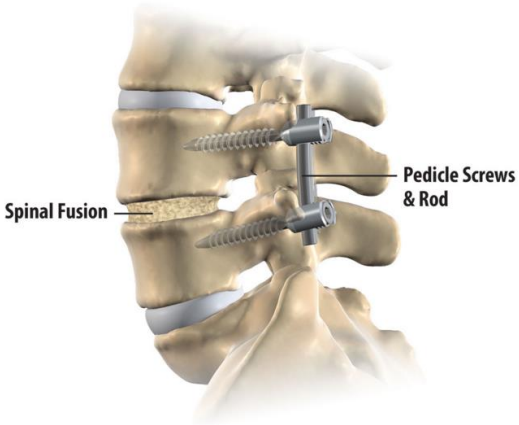

Figure 4 - Spinal Fusion (Spinal Simplicity, 2015)

The mechanical implants used are single or dual spinal rods, or spinal plates. Spinal plates (Figure 5) are used with smaller areas of interest, most notably in the cervical spine. Once fusion is completed, the surgeon places a plate across the fusion to promote stability of the joint. Cervical screws drilled into the vertebral body anchor the plate. (Scoliosis Research Society, 2015)

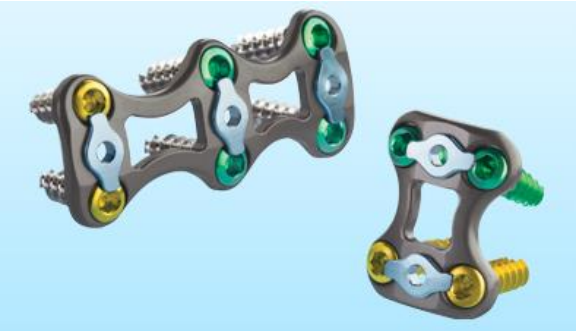

Figure 5 - Spinal Plate (Zimmer Biomet, 2014)

Spinal rods are used for correction across a larger distance, i.e. the lumbar and/or thoracic spinal regions; dual rods are used to increase spinal stability compared to single rods. After fusion of the vertebral bodies, the surgeon inserts pedicle screws into the pedicles of the vertebra. Then, one or two spinal rod(s) are curved to the desired kyphosis (natural curvature of the cervical and thoracic spine) and/or lordosis (natural curvature of the lumber spine). The spinal column is pulled towards the rods, and set screws are used to maintain the location of the spinal column and spinal rod(s). (Scoliosis Research Society, 2015)

The single and dual rod implants are compared mechanically through the American Society for Testing and Materials (ASTM) International F1717 standard (Figure 6). The F1717 standard provides procedures on how to compare different materials mechanically through compression, fatigue, and torque testing.

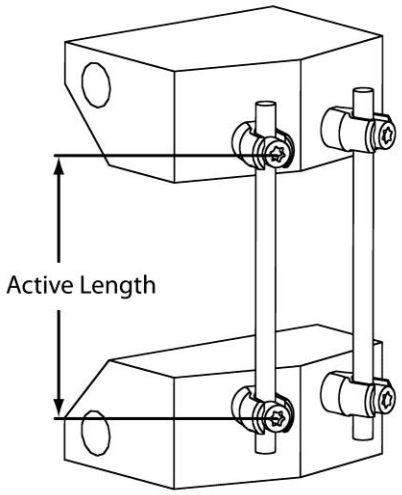

Figure 6 - F1717 Construct

1.3 – Current Knowledge and Design – Pediatric

EOS population has three typical surgical options: (1) definitive fusion, (2) guided growth systems, or (3) distraction-based systems (Skaggs, Akbarnia, Flynn, Myung, Sponseller, & Vitale, 2014). Definitive fusion involves the fusion of vertebrae with the goal of stopping the progression of the scoliotic curvature (Skaggs, Akbarnia, Flynn, Myung, Sponseller, & Vitale, 2014). When fusion is applied in EOS patients there is risk for long-term pulmonary complications due to restricted growth of the spinal column.

Guided growth systems are surgeries with multiple vertebrae anchored to rods. Guide growth systems include Luque Trolley and Shilla. Guided growth systems have been found to cause fusion of the spine within the constructs. (Skaggs, Akbarnia, Flynn, Myung, Sponseller, & Vitale, 2014)

Distraction-based systems are surgeries that apply distractive forces across the deformed spinal segments with anchors at the top and bottom of the mechanical implants. Distraction-based systems include growing-rods, vertical expandable titanium rib prosthesis (VEPTR), and hybrid growing-rods. The growing-rod implant uses a system that is rib- or spinal-based in which the vertebral bodies are supported and guided to correction of curvature with growth-friendly rods. The growth-friendly rods consist of two in-line or parallel rods that

give rise to a ‘singular’ growing-rod implant that allows controlled growth. (Skaggs, Akbarnia, Flynn, Myung, Sponseller, & Vitale, 2014)

Of these surgical procedures, the growing-rod implant is the only one that permits continued growth of the spine without fusion and minimizing the negative outcomes. Without the continued growth of the spinal column, there are a multitude of negative effects of lung development, trunk growth, and mortality due to respiratory or cardiovascular disease (Pehrsson, Larsson, Oden, & Nachemson, 1992).

The growing-rod implant is used to assist in correcting severe Cobb angles in the EOS patient population. The growing-rod implant is composed of spinal rods with rod-connectors and spinal anchors (pedicle screws or hooks). These spinal rods are curved to the desired kyphosis and/or lordosis, according to patient needs, and connectors connect the superior and inferior rods to create continuous growing rod. The anchors are positioned at the top and bottom, as well as between when and where needs of the patient are determined, of each continuous growing-rod to provide stability. Once the anchors have been inserted and the growing-rod has been contoured, the spine is pulled to align with the rods. The rods are then attached to the anchors with set screws. (Scoliosis Research Society, 2015) (Bianco, Aubin, Mac-Thiong, Wagnac, Eng, & Arnoux, 2015)

The pediatric spine is different from the adult spine in that it is still developing; the growing-rod allows the spine to grow while providing support and correcting curvature. These growing-rod constructs are known to have high failure rates. Growing rods are placed under greater demands compared standard dual rod constructs, as no fusion is preformed during surgery, and the rods are continually loaded for the life of the construct. Also, growing-rod implants are serially lengthened at six-month intervals, placing additional demands compared to standard dual rod implants (Bess, et al., 2010).

Figure 7 - Growing Rod in Patient (Scoliosis Research Society, 2015)

1.4 – Gaps in Pediatric Knowledge

Currently, there are no standards on how to evaluate the mechanics of vertebral constructs related to growing rods in pediatric patients.

1.5 – Failure Modes

Mechanical failure occurs in patients with single or dual spinal rod implants, or growing-rod implants. There are two main failures for pediatric and adult patient populations: (1) spinal rod failure, and (2) anchor failure. Complications due to implant complications (i.e. rod failure or anchor failure) are increased in pediatric patients due to less soft-tissue coverage, smaller vertebral bodies, and less physiologic reserve (Bess, et al., 2010). If either of these failures occurs, then surgical intervention is needed immediately.

Rod failure occurs when the rod yields and/or breaks – meaning the rod has lost the ability to support the normal loads of the body. Failure of the rod occurs along the length of the rod and is due to cyclic loading, i.e. fatigue. Micro-fractures on the rod, particularly where the set screws are placed, increase the probability of failure as well as speed at which failure ensues. A patient that has rod failure runs the risk of spine damage, skin abrasions, and/or metallosis. Thus, surgical intervention is necessary in order to deal with the sequelae of rod failure.

Anchor failure is one of two failures: (1) pedicle screw pullout or break, or (2) hook dislodgement. Hook dislodgement occurs when the hook detached from the rib. Pullout of a pedicle screw occurs when the pedicle screw detaches from the vertebral body. This occurs when loads from the rod and spinal column are maximized, accompanied by a weakened screw-to-bone interface. Since pediatric spines are still developing, they have softer bone compared to adolescents or young adults. Failure is due to the loads exceeding the screw-to-bone interface capacity to resist the loads. The loads are maximized near the ends of the rod, particularly when rods are applied with a kyphosis/lordosis curve. Like rod failure, pedicle screw pullout can cause spine damage, skin abrasions, and/or metallosis. Thus, surgical intervention is necessary in order to minimize the risks associated with pedicle screw pullout. Carl-Éric Aubin and his group from the Polytechnic Montreal are analyzing pedicle screw pullout, and we will focus on rod failure (Bianco, Aubin, Mac-Thiong, Wagnac, Eng, & Arnoux, 2015).

1.6 – Project Objective

The objective of this study was to develop and utilize a finite element (FE) model for standard dual constructs and growing-rod constructs based off of the current F1717 ASTM International standard, and analyze each construct with two active lengths and two spinal rod materials.

Chapter 2. Materials and Methods

The FE models were created with Abaqus CAE software at the Minnesota Supercomputing Institute (MSI). The models were meshed with C3D8R type elements, described as linear eight-node three-dimensional continuum bricks with reduced integration. The FE models determined the reaction forces and corresponding displacement at each increment determined by Abaqus CAE, i.e. the compressive bending data recommended by the ASTM International standard F1717, that depicts how and when spinal rod failure occurs. The static Riks analysis method, provided by Abaqus CAE, was used to capture the buckling behavior of the rods while displacement control was applied. The static Riks method is used to predict unstable, geometrically nonlinear collapse of a

structure. The geometrically nonlinear static problem for our models created involved buckling or collapse behavior of the constructs, where the force-displacement curves showed a negative stiffness and in order to remain in equilibrium the constructs had to release strain energy. Fatigue analysis will be determined at a later time, with the recommendation to use FE-SAFE with Abaqus CAE through MSI.

The compressive bending data collected were force-displacement curves for each simulation. From each force-displacement curve, the compressive bending ultimate load (see Point E in Figure 8), compressive bending yield load (see Point D in Figure 8), displacement at 2% offset yield (see Point A in Figure 8), 2% offset displacement (see Point B in Figure 8), elastic displacement, and ultimate displacement (see Point F in Figure 8) were determined per F1717 procedure. (ASTM Standard F1717, 2014, 1996)

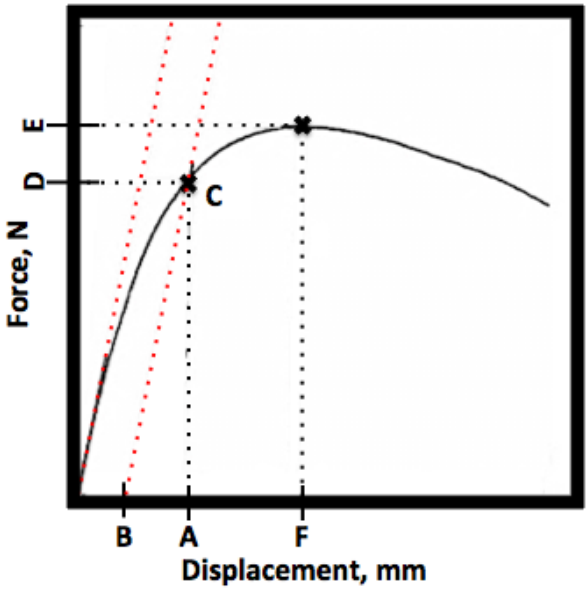

Figure 8 - Force-Displacement Curve (ASTM Standard F1717, 2014, 1996)

The ultimate load (N) is defined as the maximum compressive force. The ultimate displacement is the displacement (mm) corresponding to the ultimate load. The yield load (N) is the compressive force required to permanently deform the construct to 0.020 times the active length (the length from superior to inferior pedicle screws). The displacement (mm) at 2% offset yield is the displacement that relates to the yield load. The 2% offset displacement is equal to 0.020 times

the active length. The elastic displacement is the difference between the displacement at 2% offset yield and 2% offset displacement. (ASTM Standard F1717, 2014, 1996)

Failure criteria for the models were examined when analyzing the maximum principal stress of each model. The stress was examined for the whole model, with need to analyze failure of each part separately at a later time. The locations for the maximum and minimum stresses were located for each model to determine where failure was likely to occur. Failure was determined based off the maximum principal stress theory as well – when the principal stress exceeds the maximum normal strength of the material (i.e. $\sigma_{principal} \geq \sigma_{ultimate}$).

2.1 Parts & Materials

Each FE model was based on a combination of blocks, multi-axial pedicle screws, non-break-off set screws, connectors, domino set screws, fixtures, and spinal rods (Figure 8). There are four types of materials used to make these parts: (1) titanium alloy (Ti-6Al-4V), (2) cobalt chrome alloy (Co-28Cr-6Mo), (3) ultrahigh molecular weight polyethylene (UHMWPE), or (4) AISI 304 stainless steel. The fixtures used are incorporated to fix and apply the displacement control for the compressive bending test, restricting range of motion for the construct.

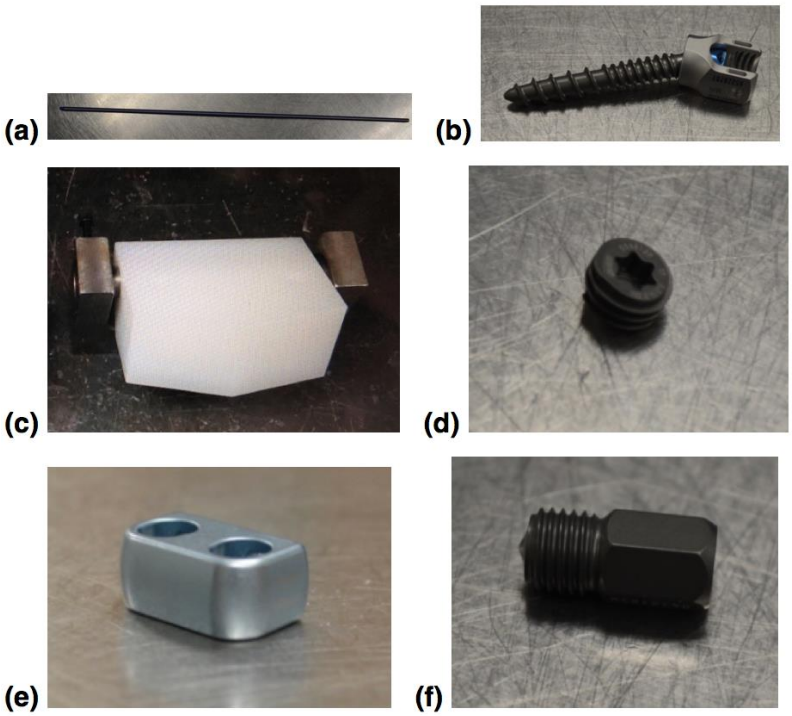

Figure 9 - (a) Spinal Rod, (b) Multi-Axial Pedicle Screw, (c) Block, (d) Non-Break-Off Set Screw, (e) Connector, and (f) Domino Set Screw

The materials are defined through tensile properties from current ASTM International standards F136 (wrought Ti-6Al-4V) and F1537 (wrought Co-28Cr-6Mo). The remaining material properties were obtained from the Material Properties Database and Aerospace Specification Metals, Incorporation (ASM). The material properties are listed in Table 1.

Table 1 - Nominal Material Properties (ASTM Standard F136, 2013, 1984) (ASTM Standard F1537, 2011, 1984)

	Ti-6Al-4V	Co-28Cr-6Mo	UHMWPE	Steel
Mass Density, tonne/mm^3	4.38×10^{-9}	8.3×10^{-9}	9.4×10^{-10}	8×10^{-6}
Young's Modulus, MPa	110,000	210,000	800	200,000
Poisson's Ratio	0.342	0.4	0.46	0.29
Yield Strength (0.02%-offset), MPa	920	560	---	---
Tensile Strength, MPa	1,020	980	49	---
Elongation – Strain, %	11	25	400	---

The stresses and strains seen in Table 1 are provided as nominal (or engineering) values. Abaqus CAE requires the true stress and plastic strain

values, so the values from Table 1 were converted using the following equations, where σ denotes stress, ε represents strain, and E is the Young's modulus.

$$\sigma_{TRUE} = \sigma_{NOMINAL}(1 + \varepsilon_{NOMINAL}) \quad (1)$$

$$\varepsilon_{TRUE} = \ln(1 + \varepsilon_{NOMINAL}) \quad (2)$$

$$\varepsilon_{PLASTIC} = \varepsilon_{TRUE} - \frac{\sigma_{TRUE}}{E} \quad (3)$$

The converted values are shown in Table 2.

Table 2 - Abaqus Input Data, Material Properties

	Ti-6Al-4V	Co-28Cr-6Mo	UHMWPE	Steel
Mass Density, tonne/mm^3	4.38 x 10^{-9}	8.3 x 10^{-9}	9.4 x 10^{-10}	8 x 10^{-6}
Young's Modulus, MPa	110,000	210,000	800	200,000
Poisson's Ratio	0.342	0.4	0.46	0.29
Yield Strength (0.02%-offset), MPa	921.84	561.12	---	---
Tensile Strength, MPa	1,132	1225	245	---
Plastic Strain, %	9.4	21.7	130.3	---

2.2 – ASTM F1717, Dual Rod Vertebrectomy Construct

The four model designs in Abaqus CAE for the dual rod vertebrectomy model were created based on the F1717 standard (Figure 6) with regards to the specifications of the lumbar bilateral construct test setup for screws along with the lumbar bilateral UHMWPE block for screws or bolts. Each part was created and meshed independently: UHMWPE block, spinal rod, multi-axial pedicle screw head, multi-axial pedicle screw body, and fixture. Each F1717 model consisted of two blocks, four pedicle screw heads, four pedicle screw bodies, two rods, and two fixtures.

In order to assemble the FE model properly, accurate placement and constraints on the parts were necessary.

There were two types of constraints implemented on the models: (1) tie and (2) equation constraints. The tie constraints used a master and slave surfaces to create an interaction that tied the two parts together. The following pairs used tie constraints: four block and pedicle screw body constraints, two

block and fixture constraints, four pedicle screw head and pedicle screw body constraints, and four pedicle screw head and rod constraints.

The equation constraint instructed the simulation to distribute the load evenly over the top of the superior fixture with the use of a single node and follower nodes. The single node acted as a collection of the follower nodes, when applying the load to the single node, it results in evenly distributed over the follower nodes.

The boundary conditions that follow replicate the conditions of a uniaxial compression/tension test of an F1717 construct. Fixed boundary conditions were applied to the sides of the blocks and fixtures. The blocks were able to rotate about the 1-direction and move in the 2- and 3-directions, and fixed in remaining degrees of freedom. The superior fixture was constrained to movement in the 3-direction and rotation about the 1-direction. The inferior fixture was constrained to movement of rotation about the 1-direction only.

Displacement control was placed in the 3-direction on the superior fixture at the single load node. If the displacement is positive, then testing was uniaxial tension; if the displacement is negative, then testing was uniaxial compression. The displacement control was provided through change of boundary conditions during the static Riks step.

The pedicle screw body was simplified to a cylinder connected to a rectangular solid, with dimensions as seen in Figure 10. A larger screw diameter of 6.5-mm was chosen to promote rod failure. A shorter pedicle screw length requires an increase in the amount of force to bend the construct.

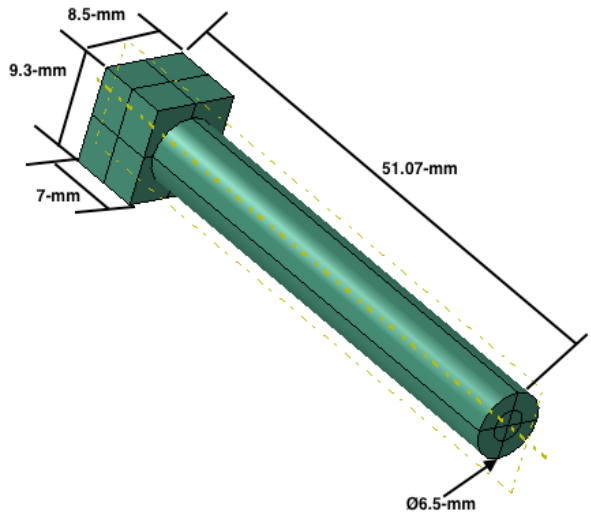

Figure 10 - Pedicle Screw Body, Dimensions

The pedicle screw head was simplified into a rectangular solid with cuts for the rod and the pedicle screw body, as can be seen in Figure 11. The separation of the head and body of the pedicle screw allows for incorporation of the degrees of freedom of the multi-axial pedicle screw; separation also provides ease in accounting for difference in material properties.

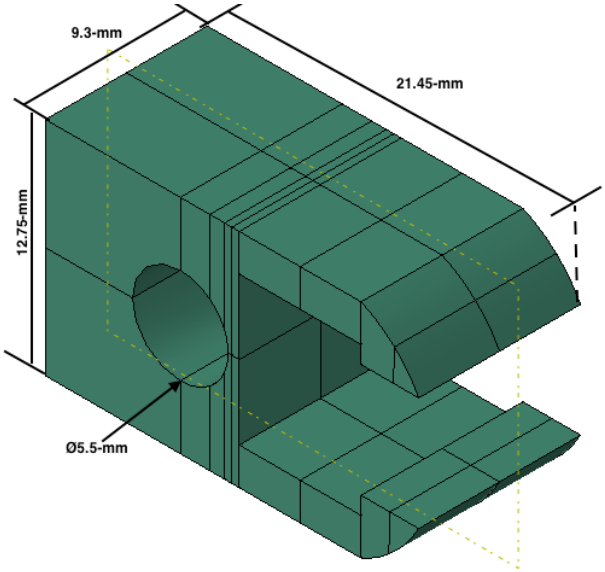

Figure 11 - Pedicle Screw Head, Dimensions

The UHMWPE block is made to mimic mature spinal vertebrae. The dimensions follow the F1717 specification for a lumbar bilateral construct, keeping note of the pilot holes diameters and the separation distance of the pilot

holes. The pilot holes were set to 6.5-mm diameters; since the model constrains the pedicle screw inside the pilot hole on the block, a true pilot hole size set to the minor diameter did not have to be considered. The separation distance was set to 40-mm, and full dimensionality is seen in Figure 12 (ASTM Standard F1717, 2014, 1996).

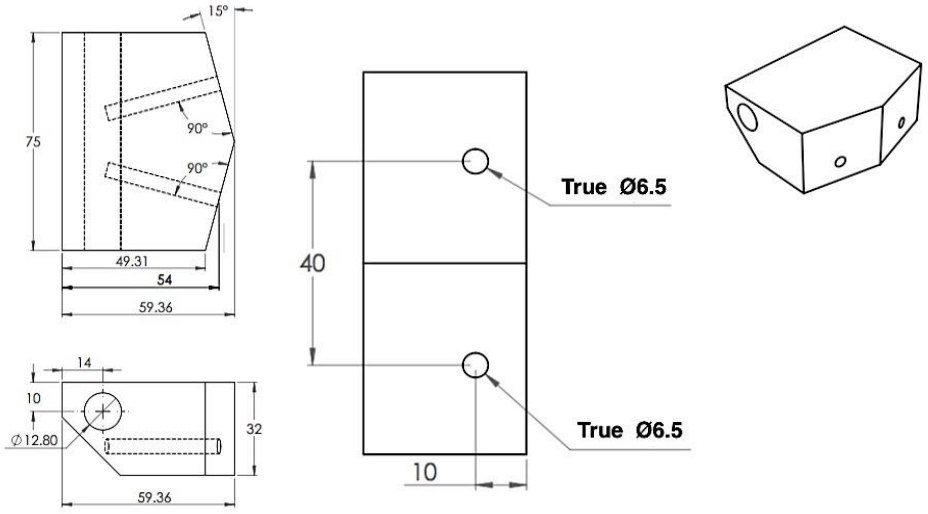

Figure 12 - UHMWPE Block Dimension (in mm)

The spinal rods were designed as cylinders with a diameter of 5.5-mm. The length of the rod depended on the active length, measured distance from superior to inferior pedicle screw (Figure 13b). The two active lengths used were 76-mm and 376-mm; each active length was tested separately with Ti-6Al-4V and Co-28Cr-6Mo spinal rods.

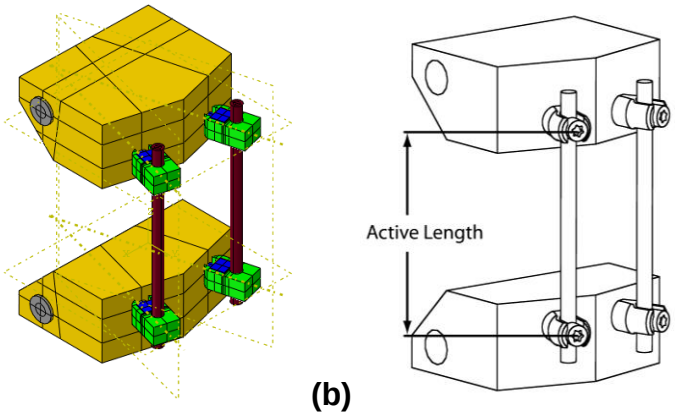

(a) **(b)**

Figure 13 - F1717 Construct (a) Abaqus and (b) Active Length

2.2.1 – Active Length, 76-mm

The first set of F1717 models had an active length of 76-mm, making the rods a length of 100-mm. The active length was chosen based off of the F1717 recommendation for a dual rod construct. The mesh was composed of 136,082 elements and 160,328 nodes. The mesh was the same for titanium and cobalt chrome rod simulations since the dimensions were consistent in both materials.

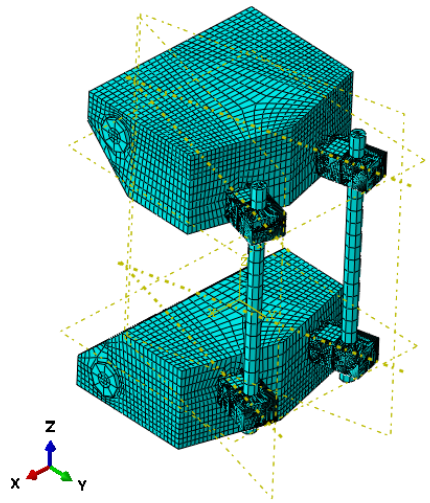

Figure 14 - Mesh of F1717, Active Length 76-mm

2.2.2 – Active Length, 376-mm

The second set of F1717 models had an active length of 376-mm, and the rods used had the length of 400-mm. The active length was chosen based off of the length of the thoracic and lumbar spine when the spine has fully matured. The mesh was composed of 138,482 element and 163,328 nodes, regardless of rod material.

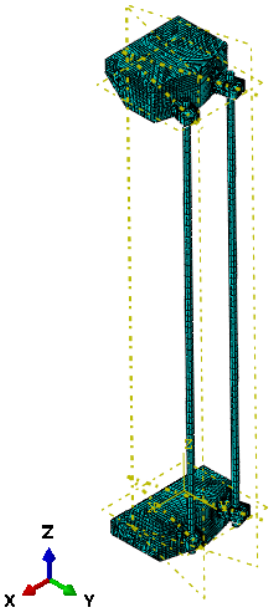

Figure 15 - Mesh of F1717, Active Length 376-mm

2.3 – Growing Rod Vertebrectomy Construct

The four models designed in Abaqus CAE for the growing rod vertebrectomy model (pediatric non-fusion device) were created with modifications made to a specific construct in the F1717 standard. The test construct used was the lumbar bilateral setup for screws. The modifications were made to the blocks used – the lumbar bilateral UHMWPE block for screws and bolts. These block modifications were made to account for the connectors, which moved the location for the pilot holes on the blocks (see Figures 17 and 18). The location of the pedicle screws allow for the same moment arm as the F1717 standard UHMWPE block. As with the F1717 models, each part of the growing-rod constructs was created and meshed independently. There is one UHMWPE superior block (Figure 17), one UHMWPE inferior block (Figure 18), two fixtures, four pedicle screw heads, four pedicle screw bodies, four rods, and two connectors (congruent to four connector when distance between connectors has been minimized, i.e. touching).

The same two types of constraints were used as in the F1717 models: the tie and equation constraints. The equation constraint is the same as the F1717 models refer to Chapter 2.1 for more details. The following pairs used the tie

constraint: four block and pedicle screw body constraints, two block and fixture constraints, four pedicle screw head and body constraints, four pedicle screw head and rod constraints, and four rod and connector constraints.

The boundary conditions, displacement control, and the pedicle screw head and body are equivalent to the process described in Chapter 2.1. See Chapter 2.1 for more information.

A simplified double connector was created as a long single connector, done to eliminate errors from misalignment of two connectors on a growing rod. A rounded rectangular solid with two holes for the rods was made for simplification of the connection. The dimensionalized part can be seen in Figure 16.

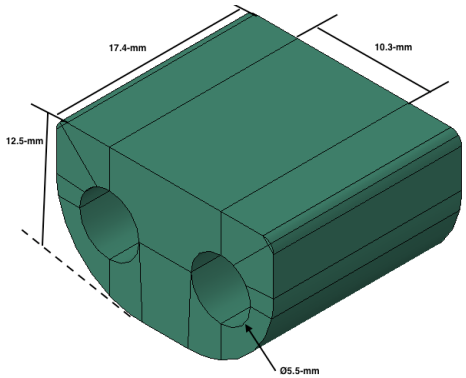

Figure 16 - Connector, Dimensions

The superior and inferior UHMWPE blocks were made to mimic mature spine vertebras, but now with the capabilities to account for side-to-side rod displacement that arose from the connectors. Thus, the separations between the pilot holes are 29.7-mm and 50.3 for the superior and inferior blocks, respectively. These were chosen to allow for the same moment arm, and displaced according to the length from diameter to diameter of the connector. See Figure 17 and 18 for full dimensionality of the superior and inferior blocks.

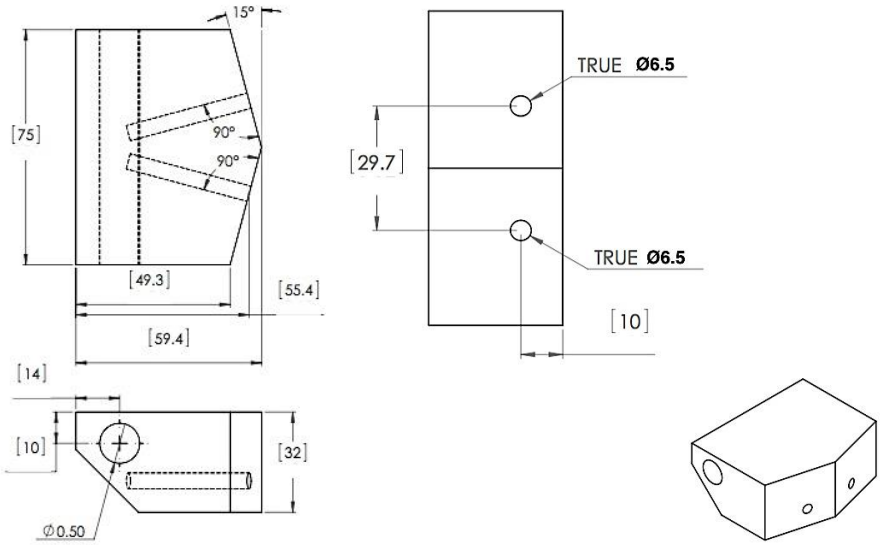

Figure 17 - UHMWPE Superior Block, Dimensions (in mm)

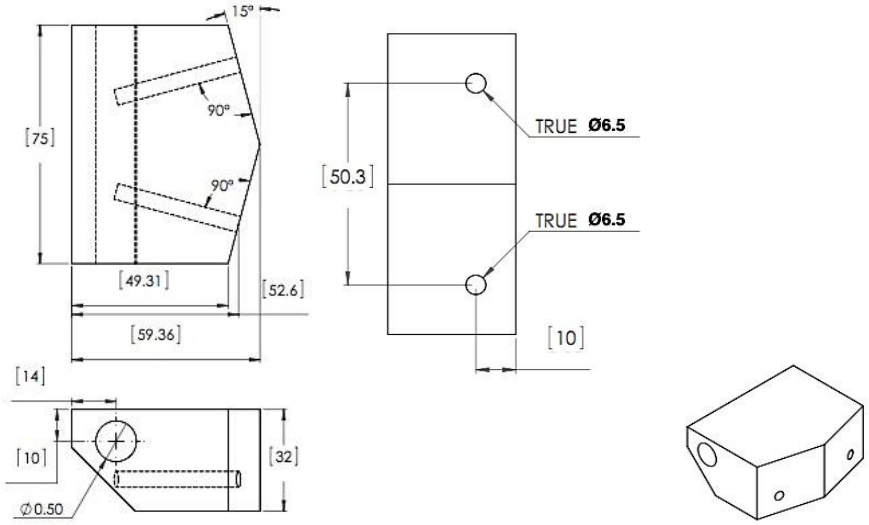

Figure 18 - UHMWPE Inferior Block, Dimensions (in mm)

The spinal rods were created as long cylinders with a diameter of 5.5-mm. The rod length was chosen based on the connector length and the active length, and then halved to account for two rods along each active length. The two active lengths were 76- and 376-mm, and for each active length the model was separately simulated with Ti-6Al-4V and Co-28Cr-6Mo spinal rods.

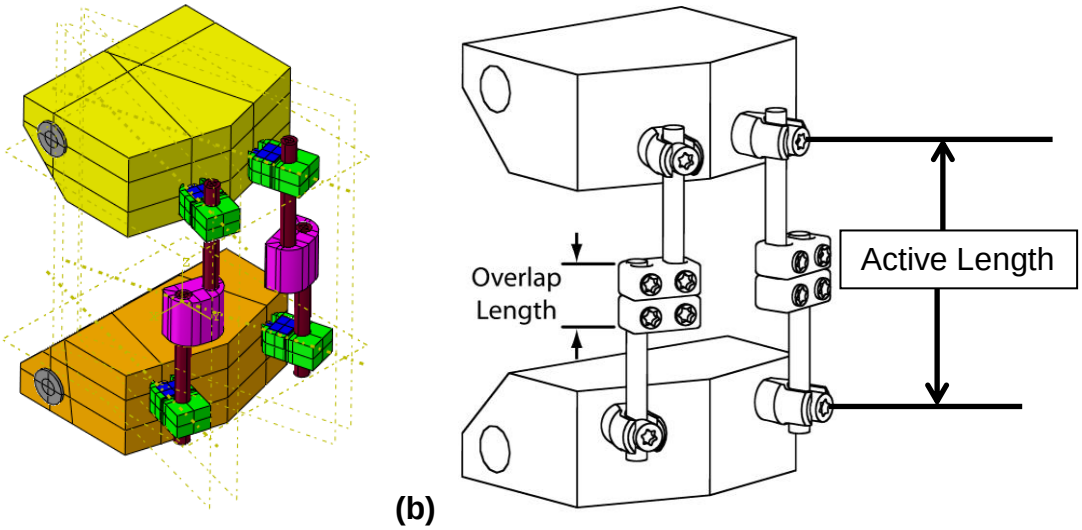

(a) **(b)**

Figure 19 - Growing-Rod Construct (a) Abaqus and (b) Active Length

2.3.1 – Active Length, 76-mm

The first set of the growing rod models had an active length of 76-mm, with a corresponding rod length of 58.7-mm. The mesh was composed of 172,146 elements and 203,491 nodes.

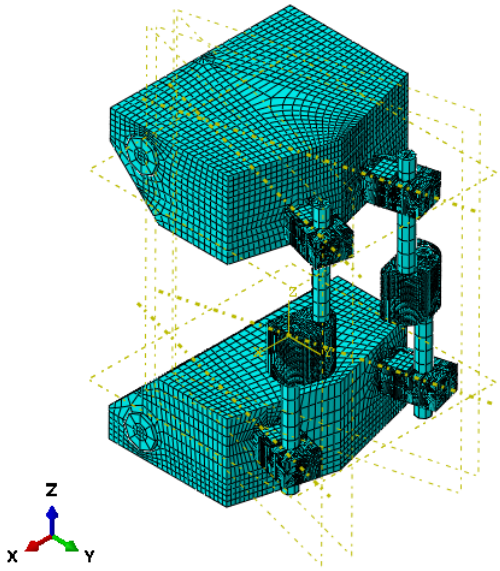

Figure 20 - Mesh of Growing-Rod Construct, Active Length 76-mm

2.3.2 – Active Length, 376-mm

The second set of growing rod models had an active length of 376-mm, with a corresponding rod length of 208.7-mm. The mesh was composed of 174,546 elements and 206,491 nodes.

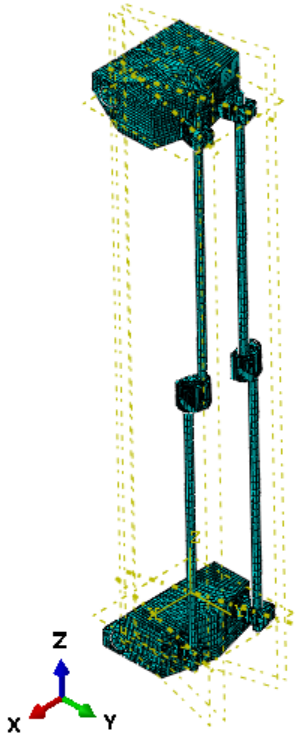

Figure 21 - Mesh of Growing-Rod Construct, Active Length 376-mm

Chapter 3. RESULTS

The following section provides details on the testing of different variables and their effects on the F1717 standard and growing rod constructs. From each force-displacement curve the compressive bending ultimate load, compressive bending yield load, displacement at 2% offset yield, 2% offset displacement, elastic displacement, and ultimate displacement were determined (see Chapter 2 for more details).

From each maximum principal stress figure from Abaqus CAE, the maximum and minimum stress points were found according to Abaqus CAE criteria.

3.1 – Material Properties Simulations

In order to check the material properties in Abaqus CAE, 10 x 10 x 10-mm blocks were simulated in compression. The stress-strain curves for titanium and cobalt chrome were evaluated, and seen in Figure 22. Stress was defined to go to 1-MPa after maximum stress occurred due to program limitations (not seen in Figure 22, only shown to increment after failure). From the stress-strain curves, it can be seen that the titanium has a higher ultimate stress (i.e. stronger), stiffer (i.e. higher Young's modulus), and brittle (i.e. low ultimate strain). Cobalt chrome is more compliant, ductile, and weaker.

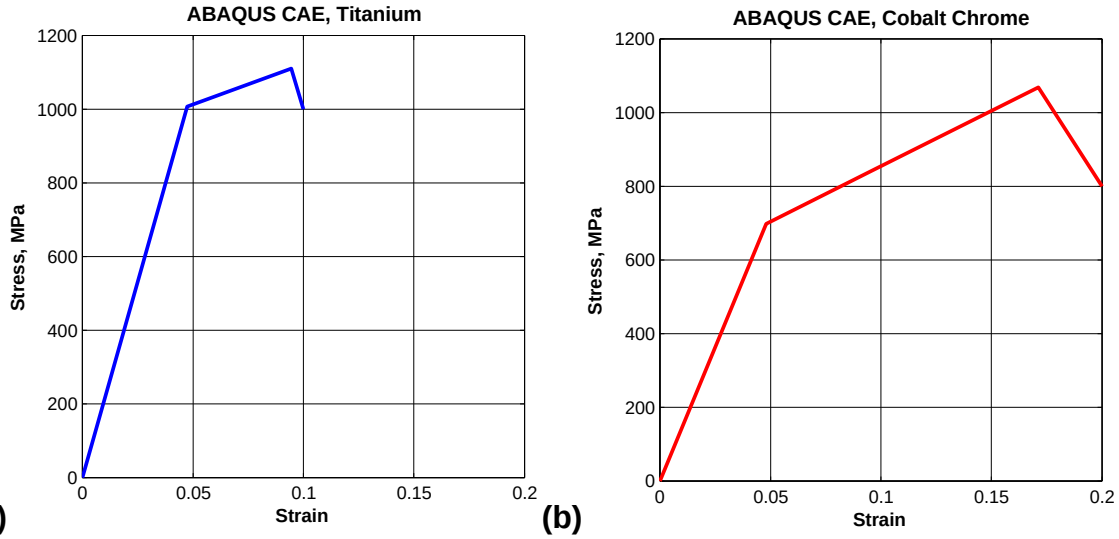

Figure 22 - Stress-Strain Curves (a) Titanium Block, and (b) Cobalt Chrome Block

3.2 – F1717 Simulation Results

3.2.1 – Active Length of 76-mm

From Figure 23 and Table 3, it can be seen that the titanium rods are stronger, with larger ultimate load, than the cobalt chrome rods. The cobalt chrome rods are more compliant and ductile compared to the titanium rods.

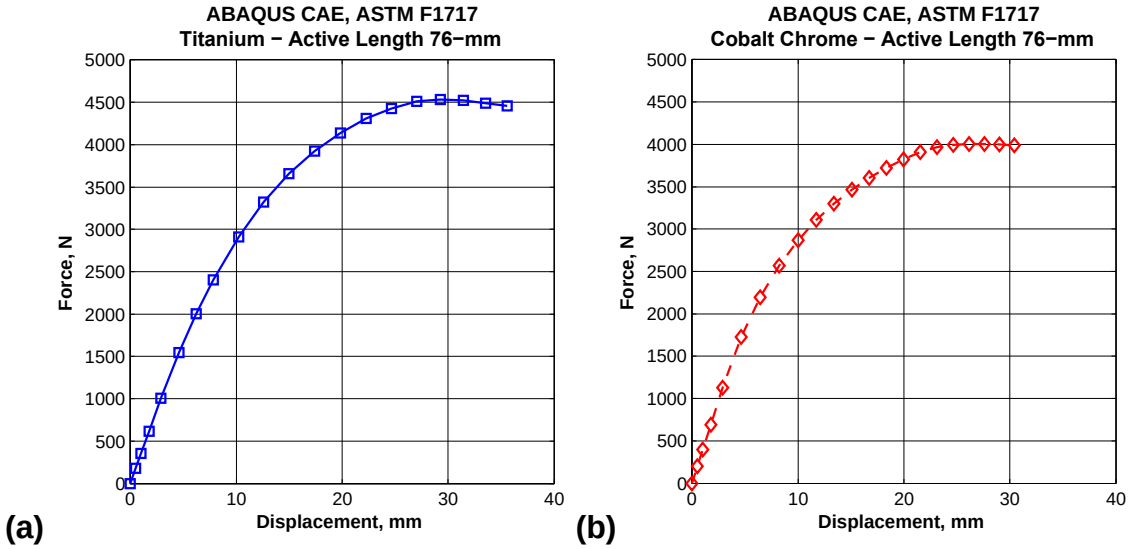

Figure 23 - Force-Displacement, F1717 Active Length 76-mm (a) Titanium and (b) Cobalt Chrome

Table 3 - F1717, Active Length 76-mm

	Ti-6Al-4V	Co-28Cr-6Mo
Ultimate Load, N	4,534.07	4,004.87
Ultimate Displacement, mm	29.28	26.14
Yield Load, N	3,000.00	2,700.00
Displacement at 2% Offset Yield, mm	11.00	9.50
2% Offset Displacement, mm	1.52	1.52
Elastic Displacement, mm	9.48	7.98

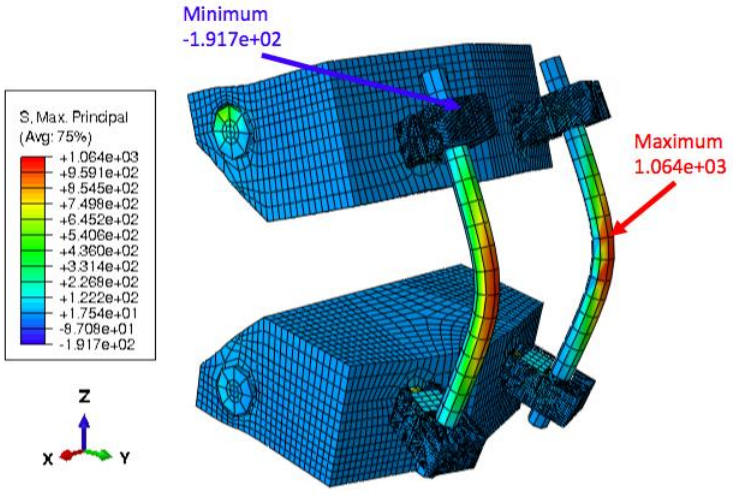

Figure 24 - Principal Stress, F1717 Titanium – Active Length of 76-mm

Figure 24 and Figure 25 depicts the maximum principal stress for the F1717 models with an active length of 76-mm and titanium and cobalt chrome rods, respectively. The minimum and maximum stress were located at the pedicle screw head and the mid-line of the spinal rod for titanium. Failure of the pedicle screw head for the titanium rods is probable since the minimum stress exceeds the absolute allowable maximum stress (Figure 24). For the cobalt chrome rods, the minimum and maximum stresses were located at the pedicle screws. The titanium pedicle screws in Figure 25 have higher minimum and maximum stresses compared to the titanium pedicle screw head and spinal rod in Figure 24. Failure in either of the titanium pedicle screws heads of the cobalt chrome rod model is feasible, since both exceed the absolute allowable maximum stress of titanium (Figure 25).

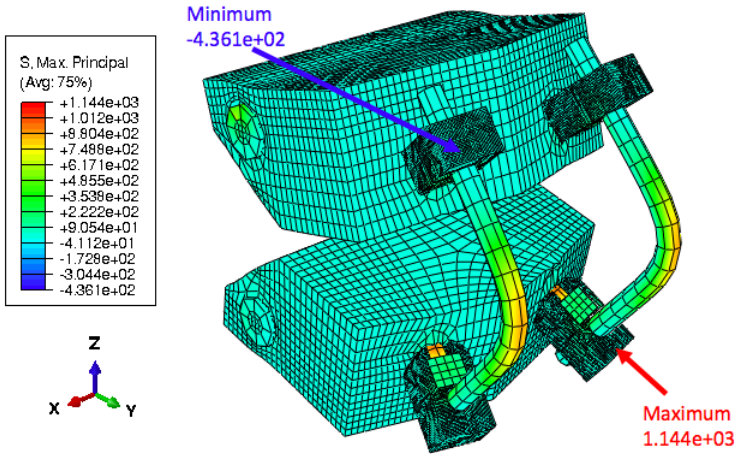

Figure 25 - Principal Stress, F1717 Cobalt Chrome – Active Length of 76-mm

3.2.2 – Active Length of 376-mm

From Figure 26 and Table 4, a larger active length, the cobalt chrome rods are stronger and more brittle compared to the titanium rods. The titanium rods are also slightly stiffer.

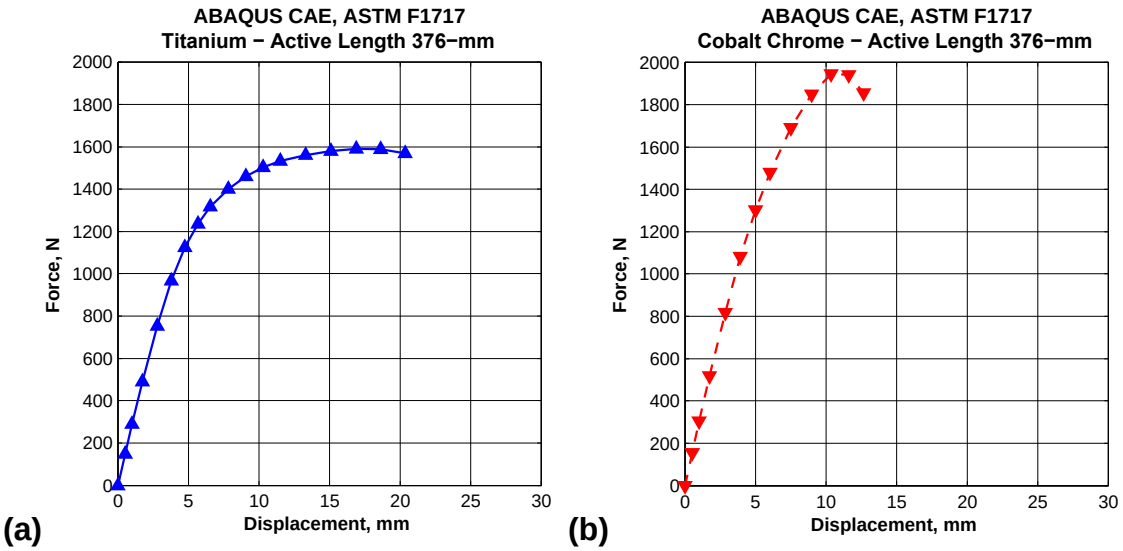

Figure 26 - Force-Displacement Curve, F1717 Active Length of 376-mm (a) Titanium and (b) Cobalt Chrome

Table 4 - F1717, Active Length 376-mm

	Ti-6Al-4V	Co-28Cr-6Mo
Ultimate Load, N	1,591.50	1,944.87
Ultimate Displacement, mm	16.88	10.35
Yield Load, N	1,580.00	1,700.00
Displacement at 2% Offset Yield, mm	15.50	14.00
2% Offset Displacement, mm	7.52	7.52
Elastic Displacement, mm	7.98	6.48

Figure 27 and Figure 28 show the maximum principal stress for the F1717 constructs with the active length of 376-mm for titanium spinal rods (Figure 27) and cobalt chrome spinal rods (Figure 28). The minimum and maximum stresses were located at one pedicle screw head for the titanium spinal rods (Figure 27).

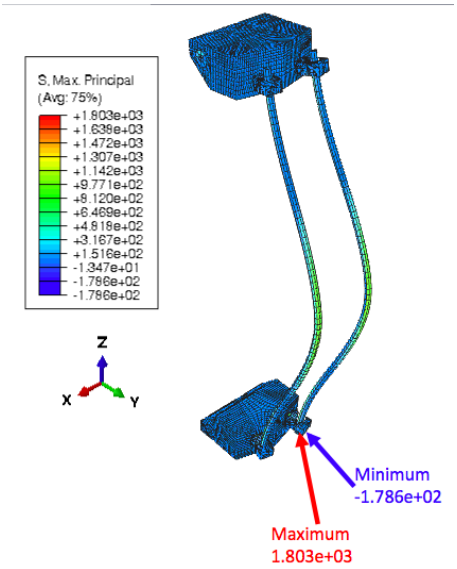

Figure 27 - Principal Stress, F1717 Titanium – Active Length 376-mm

The minimum and maximum stresses, for the cobalt chrome rods (Figure 28), were located on the superior-right and inferior-left pedicle screw heads. The titanium pedicle screw heads have a higher absolute maximum stress for the titanium spinal rod model compared to the cobalt chrome rod model. In both cases there is a high feasibility of failure of the titanium pedicle screw heads, since the absolute maximum and minimum stress exceed the ultimate stress allowed for titanium.

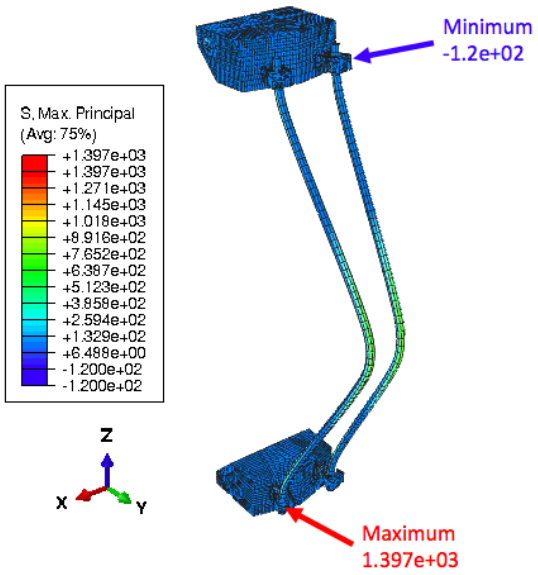

Figure 28 - Principal Stress, F1717 Cobalt Chrome – Active Length 376-mm

3.3 – Growing Rod Simulation Results

3.3.1 – Active Length of 76-mm

An interesting note in the results from Figure 29 is that an ultimate load did not occur for the cobalt chrome rods with an active length of 76-mm. There is also a toe region in both models, which is more pronounced in the titanium rods. Both the cobalt chrome and titanium have approximately equal stiffness.

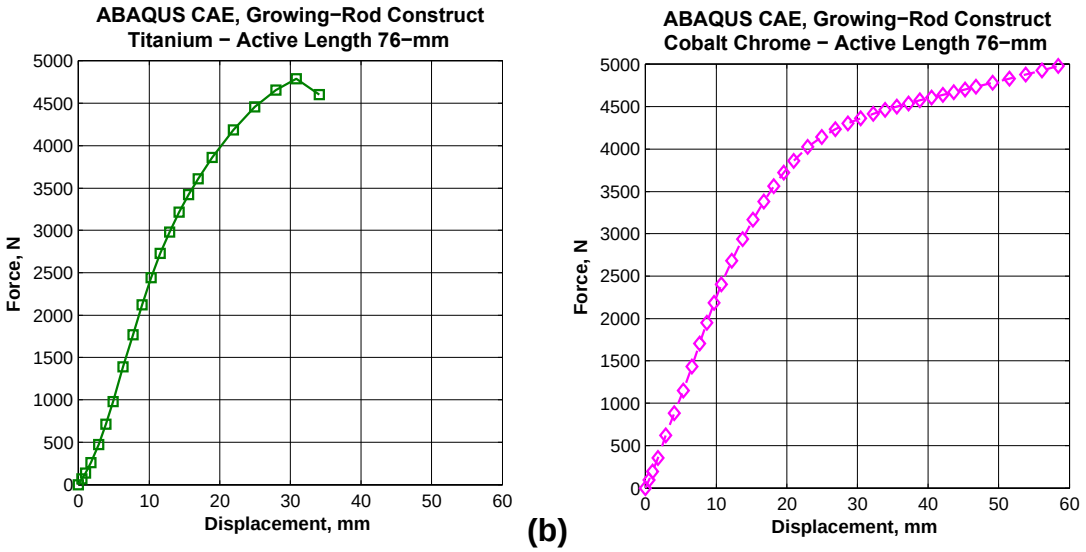

Figure 29 - Force-Displacement, Growing-Rod Active Length 76-mm (a) Titanium and (b) Cobalt Chrome

Table 5 - Growing-Rod, Active Length 76-mm

	Ti-6Al-4V	Co-28Cr-6Mo
Ultimate Load, N	4,791.55	NONE
Ultimate Displacement, mm	30.81	NONE
Yield Load, N	3,605.00	3,000.00
Displacement at 2% Offset Yield, mm	17.00	14.00
2% Offset Displacement, mm	1.52	1.52
Elastic Displacement, mm	15.48	12.48

Figure 30 and 31 show the maximum principal stresses for the growing-rod constructs with an active length of 76-mm for titanium (Figure 30) and cobalt chrome (Figure 31) spinal rods. The ultimate maximum stress for the titanium spinal rods model was found to be on the fixture, which was not given failure criteria. The ultimate minimum stress was located on the superior spinal rod

(further analysis showed the location to be at the center of the rod). Thus, the failure was likely to have occurs on the titanium spinal rod since the absolute stress surpassed the maximum allowable stress defined by the material properties for titanium.

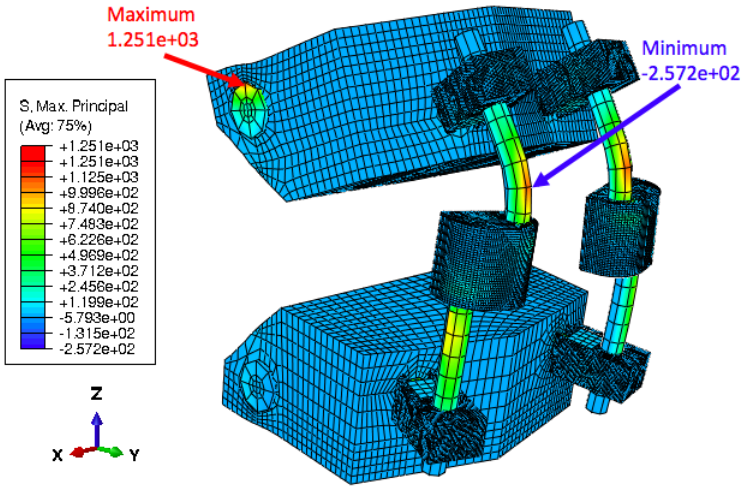

Figure 30 - Principal Stress, Growing Rod Titanium – Active Length 76-mm

The maximum and minimum principal stresses for the growing-rod cobalt chrome model (Figure 31) were located at the superior pedicle screw head and rod connectors. The maximum and minimum stresses exceeded the ones in the titanium spinal rod model above. The titanium pedicle screw head and rod connector experience larger absolute stresses compared to the ultimate stress allowed for titanium, therefore failure is probable at the pedicle screw head and rod connector.

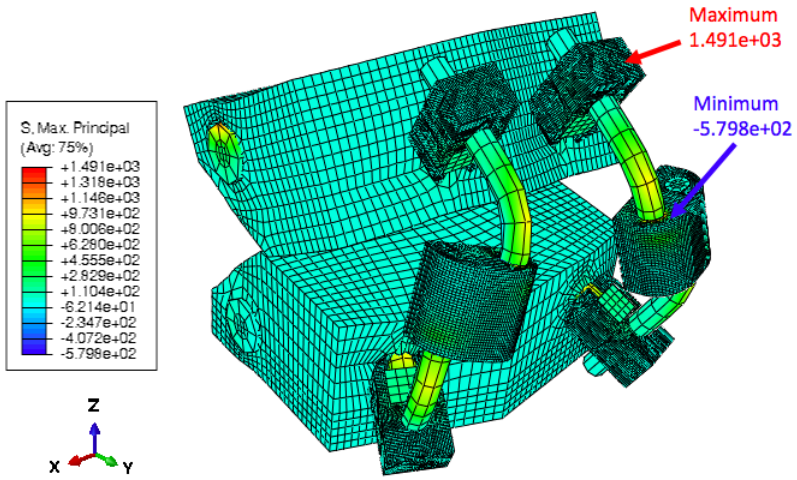

Figure 31 - Principal Stress, Growing Rod Cobalt Chrome – Active Length 76-mm

3.3.2 – Active Length of 376-mm

From Figure 32 and Table 6, growing-rods with the active length of 376-mm the cobalt chrome rods are strong and brittle, while the titanium rods are weaker and ductile. The titanium rods are also more compliant compared to the cobalt chrome rods.

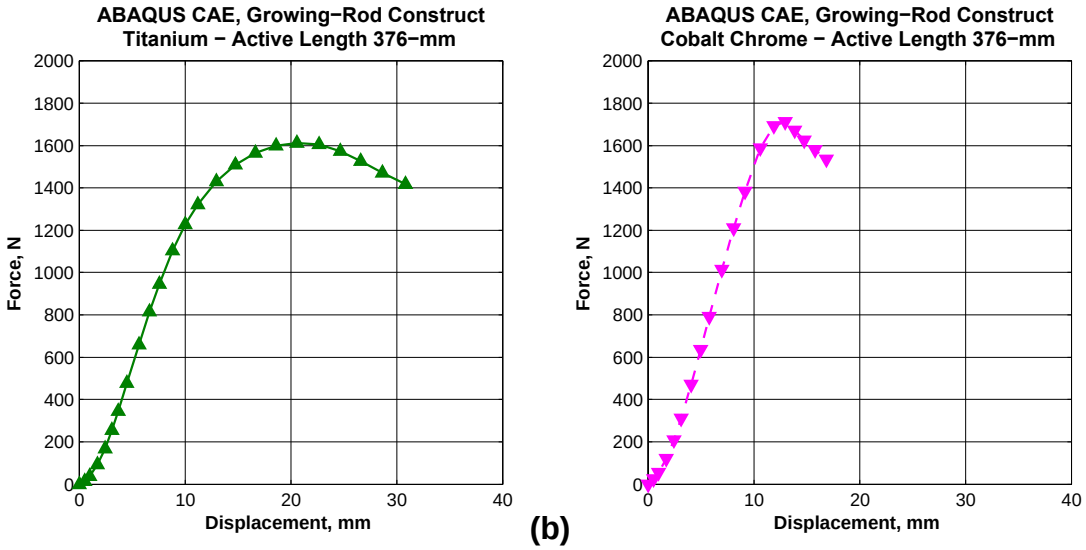

Figure 32 - Force-Displacement, Growing-Rod Active Length of 376-mm (a) Titanium and (b) Cobalt Chrome

Table 6 - Growing-Rod, Active Length 376-mm

	Ti-6Al-4V	Co-28Cr-6Mo
Ultimate Load, N	1,612.17	1,712.50
Ultimate Displacement, mm	20.56	12.95
Yield Load, N	1,575.00	1,550.00
Displacement at 2% Offset Yield, mm	18.00	16.00
2% Offset Displacement, mm	7.52	7.52
Elastic Displacement, mm	10.48	8.48

Figure 33 and 34 display the maximum principal stresses of the growing-rod constructs with an active length of 376-mm for titanium (Figure 33) and cobalt chrome (Figure 34) spinal rods. The maximum and minimum stresses occur on the superior-right and inferior-left pedicle screw head.

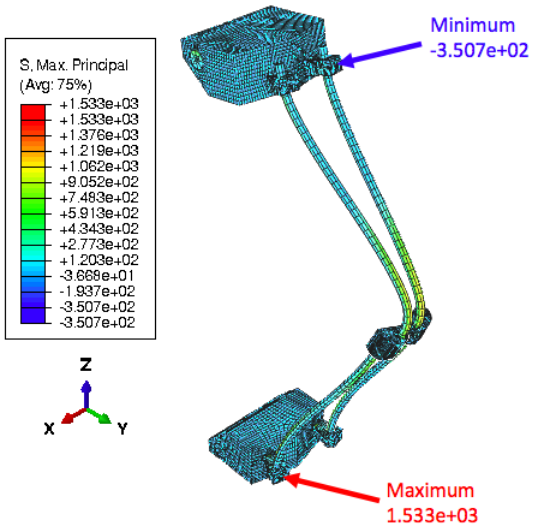

Figure 33 - Principal Stress, Growing Rod Titanium – Active Length 376-mm

The minimum and maximum stresses, for the cobalt chrome rods (Figure 34), were located on a single pedicle screw head. The titanium pedicle screw heads have a higher maximum and lower minimum stress for the titanium spinal rod model compared to the cobalt chrome rod model. In both cases there is a high probability of failure of the titanium pedicle screw heads, since the absolute maximum and minimum stress exceed the ultimate stress allowed for titanium.

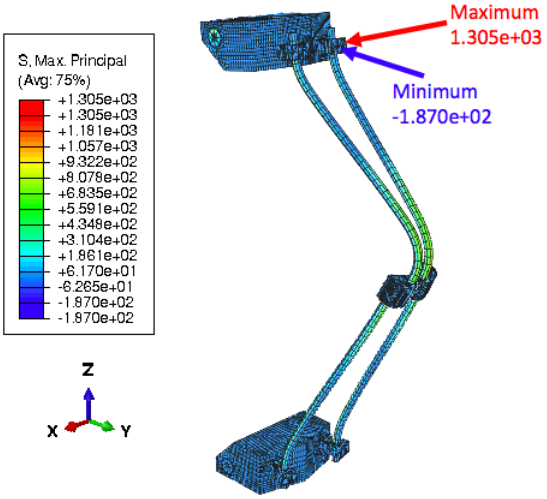

Figure 34 - Principal Stress, Growing Rod Cobalt Chrome – Active Length 376-mm

Chapter 4. DISCUSSION

The difference between the standard dual and growing-rod constructs can be determined from the FE models constructed for compressive bending. Material properties can also be altered with ease in the models, to show how the constructs change according to the type of material used with a specific part. There were a total of 8 FE models created with a combination of constructs, rod material, and active length.

These models provided the ability to see a multitude of combinations with ease and assist in determining construct specifications to base a new ASTM International standard on. Thus, providing a guideline on which to determine the best materials and design for each unique patient.

4.1 – F1717 Comparison

When looking at both active lengths for F1717 (Figure 35), the properties of the rods have reversed excluding the compliance of the constructs. The titanium rods went from brittle and strong to ductile and weak with an increase in active length. The cobalt chrome rods went from ductile and weak to brittle and strong with an increase in active length. The load also increased with a decrease the in active length, corresponding to the moment arm.

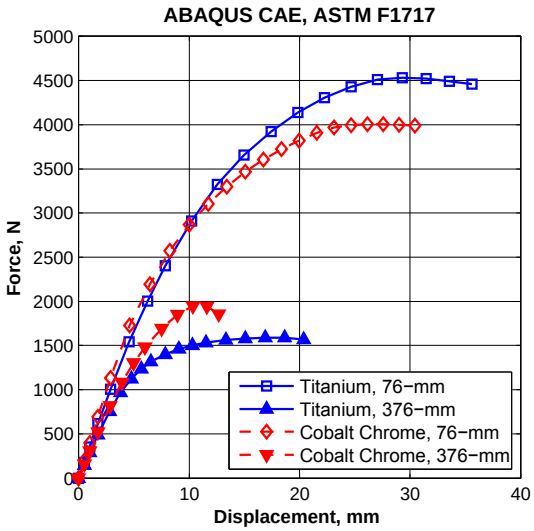

Figure 35 - F1717 Constructs, Comparison

4.2 – Growing-Rod Comparison

Figure 36 shows the two active lengths and two materials used for the rods for the growing-rod constructs. The titanium was more ductile with the increase in active length, but weaker than the cobalt chrome for both active lengths. The toe region was more defined in the longer lengths, likely due to the interaction with the connectors.

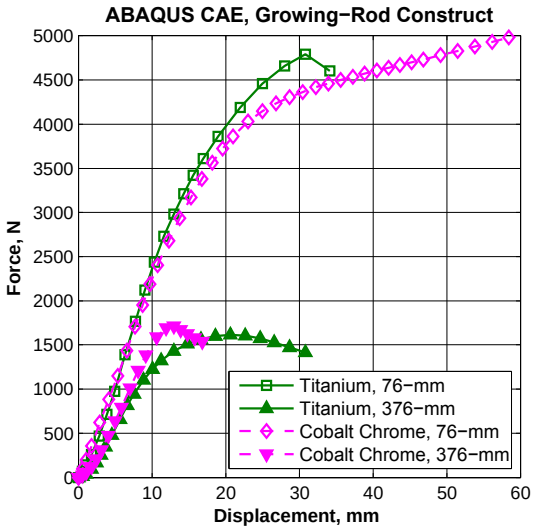

Figure 36 - Growing-Rod Constructs, Comparison

4.3 – Active Length 76-mm Comparison

Figure 37 compares both the F1717 and growing-rod constructs at an active length of 76-mm. The ductility process starts later during displacement.

The toe region causes a delay in compliance of the growing-rod constructs. The linear region is more linear in the growing-rod constructs.

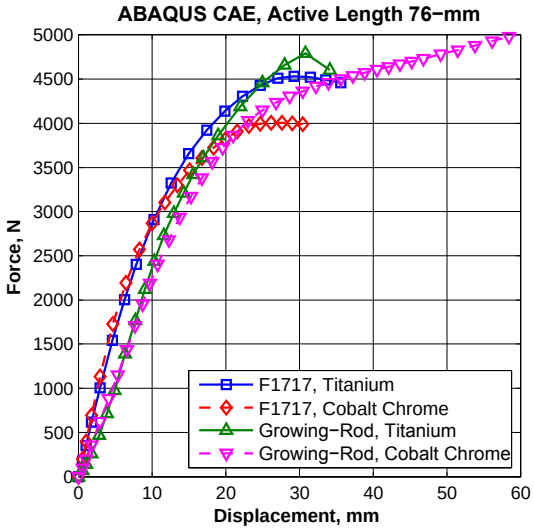

Figure 37 - Active Length of 76-mm, Comparison

4.4 – Active Length 376-mm Comparison

Figure 38 compares the growing-rod and F1717 constructs with the active length of 376-mm. The increase in active length has similarity of the F1717 and growing-rod constructs with the brittleness and strength of the constructs. There was delay in displacement for the growing-rod constructs, due to the toe region.

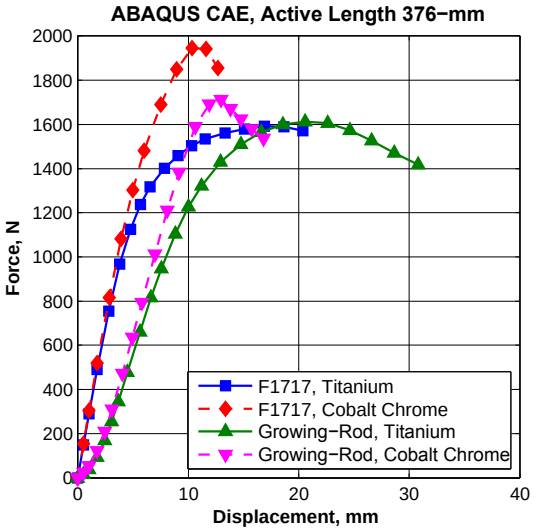

Figure 38 - Active Length of 376-mm, Comparison

4.5 – Failure Locations

Across all the models created, a commonality found is that failure of the pedicle screw head is a high probability for any variation of the model. Failure at the spinal rod for the F1717 and growing-rod constructs with active lengths of 76-mm and titanium spinal rods; rod connectors failure also occurred for the growing-rod construct with cobalt chrome rods and an active length of 76-mm.

Chapter 5. CONCLUSION

There are two types of limitations that should be noted: (1) model limitations due to simplifications, and (2) model limitations with clinical scenarios. Simplifications to the FE models were made to build off of in further research. These include a simplified pedicle screw body-to-head that included the set screw within the head. The simplified pedicle screw body does not include the threads without threads, creating perfect screw fixation. There is also perfect screw-to-rod fixation due to the combination of the pedicle screw head and set screw. Improvements should be done to include a separate set screw from the pedicle screw head, with a preload – similar to the loads applied clinically – applied to the set screw. Thread inclusion does not need to be included since promotion of rod failure is the goal of these models.

Limitations of the model compared to the clinical scenario include the loading pattern and rod contouring. The loading patterns in clinical scenarios are through cyclic loading of the constructs. The model will be used with cyclic loading at a later time, using a percentage of the ultimate loads determined.

Rod contouring is done in clinical scenarios by bending the rods to the patient needs. This contouring is known to change the material properties of the rods and includes notching of the constructs, which promote failure at the notches. The rods are assumed to be straight for the F1717 and growing-rod constructs, looking into the material properties and affects of contouring should be done as a separate mechanically tested study.

The conclusion is that the new protocol for ASTM International should include information on the toe region in growing-rod constructs. The

recommended active length should also be adjusted to account for the toe region and promotion of failure. Reviewing the placement of the connectors should be done as well, since the connectors may not always be centered for the pediatric patients.

Maximum principal stress analysis should be done for each part, determining failure possibilities of each part.

Using this computation data, comparison to mechanical data testing should be done. After FE model validation, FE models for fatiguing will be done using FE-SAFE.

Bibliography

ASTM Standard F136, 2013. (1984). Standard Specification for Wrought Titanium-6Aluminum-4Vanadium ELI (Extra Low Interstitial) Alloy for Surgical Implant Applications (UNS R56401). West Coshohocken, PA.

ASTM Standard F1537, 2011. (1984). Standard Specification for Wrought Cobalt-28Chromium-6Molybdenum ALloys for Surgical Implants (UNS R31537, UNS R31538, and UNS R31539). *ASTM International*. West Conshohocken, PA.

ASTM Standard F1582, 2003. (1998). Standard Terminology Relating to Spinal Implants. *ASTM International*. West Conshohocken, PA.

ASTM Standard F1717, 2014. (1996). Standard Test for Spinal Implant Constructs in a Vertebrectomy Model. *ASTM International*. West Conshohocken, PA, PA.

Bess, S., Akbarnia, B. A., Thompson, G. H., Sponseller, P. D., Shah, S. A., Sebaie, H. E., et al. (2010, November 3). Complications of Growing-Rod Treatment for Early-Onset Scoliosis. *The Journal of Bone & Joint Surgery, Inc., 92*(A), 2533-2543.

Bianco, R., Aubin, C., Mac-Thiong, J., Wagnac, E., Eng, P., & Arnoux, P. (2015, November). Pedicle Screw Fixation Under Non-Axial Loads: A Cadaveric Study. *Spine*.

Cunin, V. (2015). Early-onset scoliosis - Current treatment. *Orthopaedics & Traumatology: Surgery & Research, 101*, S109-S118.

Mayo Foundation for Medical Education and Research. (2015). *Mayo Clinic*. Retrieved November 2015, from www.mayoclinic.org

Pehrsson, K., Larsson, S., Oden, A., & Nachemson, A. (1992, November 9). Long-Term Follow-Up of Patients with Untreated Scoliosis: A Study of Mortality, Causes of Death, and Symptoms. *Spine, 17*, 1091-1096.

Scoliosis Research Society. (2015). *Scoliosis Research Society (SRS)*. Retrieved July 27, 2015, from www.srs.org

Skaggs, D. L., Akbarnia, B. A., Flynn, J. M., Myung, K. S., Sponseller, P. D., & Vitale, M. G. (2014, April/May). A Classification of Growth Friendly Spine Implants. *Journal of Pediatric Orthopaedics, 34*(3), 260-274.

Spinal Simplicity. (2015). *Spinal Simplicity. Innovative simple solutions.* Retrieved November 2015, from www.spinalsimplicity.com

Zimmer Biomet. (2014). *Zimmer. Personal Fit. Renewed Life.* Retrieved November 2015, from www.zimmer.com